ELSEVIER

Journal of Organometallic Chemistry 632 (2001) 94–106

Journal of Organometallic Chemistry

www.elsevier.com/locate/jorganchem

Metal–metal interaction in polynuclear complexes with cyanide bridges: synthesis, characterisation, and theoretical studies

Maria J. Calhorda [a,c], Michael G.B. Drew [b], Vitor Félix [d], Luís P. Fonseca [c], Carla A. Gamelas [c,e], Sofia S.M.C. Godinho [c], Isabel S. Gonçalves [c,d], E. Hunstock [c], João P. Lopes [c], A. Jorge Parola [f], Fernando Pina [f], Carlos C. Romão [c,*], A. Gil Santos [f]

[a] *Departamento de Química e Bioquímica, Faculdade de Ciências, Universidade de Lisboa, 1749-016 Lisbon, Portugal*
[b] *Department of Chemistry, University of Reading, Whiteknights, Reading RG6 6AD, UK*
[c] *Instituto de Tecnologia Química e Biológica da Universidade Nova de Lisboa, Quinta do Marquês, EAN, Apartado 127, 2781-901 Oeiras, Portugal*
[d] *Departamento de Química, Universidade de Aveiro, 3810-193 Aveiro, Portugal*
[e] *Escola Superior de Tecnologia, Instituto Politécnico de Setúbal, 2900 Setúbal, Portugal*
[f] *Departamento de Química, Centro de Química Fina e Biotecnologia, Faculdade de Ciências e Tecnologia, Universidade Nova de Lisboa, 2825 Monte de Caparica, Portugal*

Received 20 February 2001; accepted 17 April 2001

Dedicated to Professor Dr Alberto Romão Dias on the occasion of his 60th birthday

Abstract

The reaction of the cyanide anion $[M(CO)_5CN]^-$ (M = Cr or Mo) with metallocenes of Groups 4 and 6 produced polynuclear complexes of the type $[CpCp'M(CO)\{-NC-M'(CO)_5\}]BF_4$ (M = Mo, W; M′ = Mo, Cr; Cp′ = Cp, Ind), $Cp_2TiCl\{-NC-Mo(CO)_5\}$ and $Cp_2Ti\{-NC-Mo(CO)_5\}_2$. These complexes were characterised by ^{1}H-, ^{13}C- and ^{95}Mo-NMR, IR and UV–vis spectroscopies, elemental analysis and examined by cyclic voltammetry. These methods show that the $[M(CO)_5CN]^-$ ligands shift the electron density towards the metallocene centres. The complex $[Cp_2W(CO)\{-NC-Mo(CO)_5\}]^+$ is additionally examined by single crystal X-ray structure determination. The Density Functional Theory (DFT) calculations with the ADF program were performed on selected compounds to understand the nature of the redox processes taking place. Compared with a nitrile, the coordination of a $[M(CO)_5CN]^-$ fragment to the metallocene moiety does not significantly change the geometrical features, but leads to the stabilisation of the HOMO of the latter, with all the oxidation processes occurring in the pentacarbonyl moiety of the binuclear species. Time-dependent DFT calculations were used to identify the band appearing in the visible spectrum of $Cp_2TiCl\{-NC-Mo(CO)_5\}$ as a Mo to Ti charge transfer.

Keywords: Metallocenes; Polynuclear complexes; Cyanide bridges; Theoretical studies; DFT calculations

1. Introduction

The pioneering work by Dias and Green established the Group 6 metallocene derivatives as important organometallic ligands in the earlier days of the fast expanding scenario of organometallic chemistry [1a–d]. The search for metal–metal interactions and the modelling of Mo-containing metalloproteins and catalysts was the goal in those studies. Later studies confirmed the validity of the concept and many other organometallic ligands were explored in many different fields as building blocks for the polynuclear complexes [1e,f].

Among these, cyanide-bridged polynuclear complexes have been the centre of an extended and varied research activity spanning across many fundamental themes and applied goals. In a recent critical review Vahrenkamp put all these aspects in perspective and drew some

* Corresponding author. Tel.: +351-214418407; fax: +351-214411277.
E-mail address: ccr@itqb.unl.pt (C.C. Romão).

0022-328X/01/$ - see front matter
PII: S0022-328X(01)00849-X

guidelines for the future development of this rich field [1g–i]. With our research interests on metallocene chemistry initiated in the 1970s under the guidance of Dias [2], and more recently, on polynuclear complexes between metals in high- and low-oxidation states [3] we became interested in exploring the chemistry and properties (electron-transfer, electrochemistry, and photochemistry) of stable metallocene derivatives (M = Mo, W, Ti) containing cyanide bridges to other organometallic fragments (Cp'_2M–NC–M′Ln) of which only a few examples have been structurally characterised, namely $Cp_2Ti\{NCMn(CO)_2Cp\}_2$ [4] and $\{Cp_2Ti[(NCRu(CN)_5]_2\}^{6-}$ [5]. The use of indenyl substituted Group 6 metallocenes that facilitates the increase of the number of available oxidation states of the IndCpM fragment [6] could provide for interesting intramolecular interactions between both the metal centres observed until now and by Green and co-workers for the $Cp_2Nb(SR)_2M'Xn$ complexes [7].

The Group 6 metallocene fragments Cp'_2M (Cp′ = Cp, Ind; M = Mo, W) coordinate a host of ligands, many of which are isoelectronic with the cyanide ion, namely nitriles, isonitriles, and CO (see Chart 1) [6,8,9]. Many similar complexes are also known for the Cp_2Ti fragment [9]. This prompted the use of well-known complexes $[M(CO)_5(CN)]^-$ (M = Cr, Mo, W) as ligands capable of forming cyanide bridges between a metallocene fragment and another organometallic environment. This allows us to make a direct comparison between the properties of the isostructural but not isolectronic $Cp_2Mo(IV)$ and $Cp_2Ti(IV)$ derivatives.

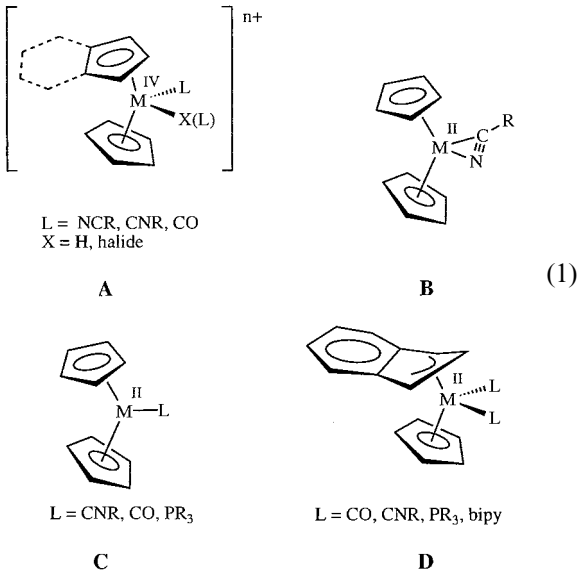

(1)

Accordingly, the present paper reports the synthesis and characterisation of a number of cyanide-bridged complexes, for both Groups 4 and 6 metallocenes, one of which, $[Cp_2W(CO)\{–NC–Mo(CO)_5\}]^+$, was crystallographically characterised. The Density Functional Theory (DFT) calculations [10] were carried out to interpret the charge transfer processes detected by UV–vis spectroscopy and the electrochemical behaviour of some representative complexes.

2. Results and discussion

2.1. Synthetic studies

The reaction of a suspension of $[Cp_2W(CO)_2][BF_4]_2$ (**1**) in dichloromethane with a solution of $Na[Mo(CO)_5CN]$ (**2**) in THF forms a good yield of the $[Cp_2W(CO)\{–NC–Mo(CO)_5\}]BF_4$ (**3**) complex. The crystal structure of **3** is described below (see Section 2.2).

This synthetic route is also used to prepare some molybdenocene derivatives $[CpCp'Mo(CO)\{–NC–Cr(CO)_5\}]BF_4$ [Cp′ = Cp (**4**), Ind (**5**)] (Scheme 1). These results show the high lability of the first leaving CO ligand as described earlier in the synthesis of $[CpCp'Mo(NCMe)(CO)]^{2+}$ and $[CpCp'Mo(NCMe)_2]^{2+}$ [6].

The ^{1}H- and ^{13}C-NMR characterisation of the compounds **3**–**5** was carried out in $NCCD_3$ at room temperature. In the ^{1}H-NMR spectra, the cations **3** and **4** show the Cp resonances as singlets at δ 6.56 and δ 6.63 ppm, respectively. These values are similar to those found for the Cp protons in the complexes $[Cp_2M(CO)_2]^{2+}$ (M = W (**1**), δ 6.46 ppm; Mo (**6**), δ 6.69 ppm) but are clearly shifted downfield relative to the acetonitrile analogues $[Cp_2M(NCMe)(CO)]^{2+}$ (M = W (**7**), δ 6.21 ppm; Mo (**8**), δ 6.32 ppm) and $[Cp_2M(NCMe)_2]^{2+}$ (M = W (**9**), δ 5.97 ppm; Mo (**10**), δ 6.05 ppm) [6]. In spite of their negative charge, the $[M(CO)_5CN]^-$ ligands are *less* donating than MeCN.

The chemical shifts of the indenyl protons for $[IndCpMo(CO)\{–NC–Cr(CO)_5\}]BF_4$ (**5**) are consistent with the typical η^5-coordination [6]. Some selected ^{13}C-NMR data for complexes **3**–**5** are listed in Table 1. The cyanide bridge in **3**–**5** is consistent with the high deshielding of the C ≡ N resonances at $\delta \approx 194$ ppm when compared with the cyanopentacarbonyl ligand, $[M(CO)_5CN]^-$ (M = Mo (**2**), δ 149.2 ppm; Cr (**11**), δ 153.8 ppm).

The infrared (IR) data of the complexes **3**–**5** in solution (MeCN) is given in Table 1. By comparison

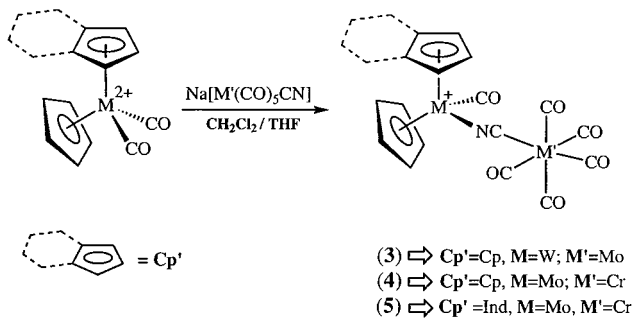

Scheme 1.

Table 1
Selected IR data [ν(C≡N), ν(C≡O), ^{13}C-NMR data ppm], and ^{95}Mo-NMR data [ppm] for the complexes prepared in this work

Compound		ν(C≡N) (cm^{-1})	ν(C≡O) (cm^{-1})	^{13}C (δ ppm)	^{95}Mo (δ ppm)
$[Cp_2W(CO)\{-NC-Mo(CO)_5\}]BF_4$	**3**	2120	2062, 2050, 1946	216.1, 209.0, 204.9 (CO), 194.5 (CN)	−1849
$[Cp_2Mo(CO)\{-NC-Cr(CO)_5\}]BF_4$	**4**	2120	2072, 2058, 1942	219.9, 216.7, 212.1 (CO), 194.9 (CN)	
$[IndCpMo(CO)\{-NC-Cr(CO)_5\}]BF_4$	**5**	2118	2068, 2058, 1942	219.9, 216.7, 213.8 (CO), 192.5 (CN)	
$Cp_2Ti\{-NC-Mo(CO)_5\}_2$	**13**	2104	−2050, 1940	208.5, 203.9 (CO), 193.7 (CN) [a]	−1831 [a]
$Cp_2TiCl\{-NC-Mo(CO)_5\}$	**14**	2106	−2048, 1946	204.4, 200.5 (CO), 182.8 (CN) [a]	−1855 [a]

All IR and NMR spectra were run in MeCN.
[a] IR and NMR spectra were run in CD_2Cl_2.

with other complexes of the $[M(CO)_5CN]^-$ ligands, we assign the ν(CO) bands at ca. 2050, 1940 cm^{-1} to this fragment. However, for all complexes only two ν(CO) bands are present the band expected at a lower energy (ca. 1860 cm^{-1}) being absent. We do not have a definitive explanation for this fact but we have previously made a similar observation for $Re_2\{\mu\text{-}O_2CC(CH_3)_3\}_4[NCM(CO)_5]$ (ν(CO) ca. 2040, 1930 cm^{-1}) [3c]. These bands show that the absorptions of ν(C≡O) are shifted to higher wavenumbers in comparison with the starting ligands $[M(CO)_5CN]^-$ [M = Mo (**2**), Cr (**11**)]. This is in agreement with the coordination of the anions to a Lewis acidic cationic centre with the concomitant removal of some electronic charge from the central zerovalent Cr or Mo atom [11]. The ν(CO) band at ca. 2070 cm^{-1} is assigned to the $[Cp'_2M(CO)]$ fragment. For example $[Cp_2Mo(CO)(NCMe)]^{2+}$ and $[IndCpMo(CO)(NCMe)]^{2+}$ show ν(CO) at 2075 and 2050 cm^{-1}, respectively [6a].

The factors that affect the ν(C≡N) frequency shifts of bridging cyanides have been discussed by several authors and the most important references can be found in the review by Vahrenkamp et al. [1g] as well as in Refs. [1g,12]. In the case of the complexes **3**–**5**, the stretching ν(C≡N) vibrations occur at higher wavenumbers relative to those of the corresponding salts $[M(CO)_5CN]^-$ (M = Mo (**2**), ν(C≡N) 2099 cm^{-1}; Cr (**11**), ν(C≡N) 2111 cm^{-1}) [3c] as expected from their coordination to a Lewis acid. The same trend is also observed in the ^{95}Mo-NMR spectrum of compound $[Cp_2W(CO)\{-NC-Mo(CO)_5\}]BF_4$ (**3**): the ^{95}Mo-NMR resonance is shifted more than 30 ppm to the lower field relative to the anion $[Mo(CO)_5(CN)]^-$ (**2**) (δ 1882 ppm, at room temperature) [3a,c]. Following the same substitution chemistry and reacting the labile acetonitrile derivatives $[Cp_2Ti(NCMe)_2][PF_6]_2$ (**12**) [13] with two equivalents of the anion $Na[Mo(CO)_5CN]$ (**2**) the trinuclear complex $Cp_2Ti\{NC-Mo(CO)_5\}_2$ (**13**) is obtained. Another binuclear complex $[Cp_2TiCl\{-NC-Mo(CO)_5\}]$ (**14**) is accessible in nearly quantitative yields after the precipitation of NaCl, from reaction of one equivalent of the pentacarbonyl ligand **2** with Cp_2TiCl_2 (**15**) [14] (Scheme 2).

The complexes **13** and **14** are more soluble in organic solvents, e.g. dichloromethane compared with the precursors **12** and **15**, and precipitate from the reaction mixture with addition of ether. They are stable at room temperature but decompose quickly in the presence of air.

The IR spectrum for these two complexes (**13** and **14**) shows the expected CO stretching vibrations as well as the typical ν(C≡N) vibration. In general, ν(C≡N) is shifted to a higher frequency upon bridge formation [12]. Indeed, in both cases (**13** and **14**) the bridging cyanide group exhibits approximately the same absorption frequency as the terminal cyanide group $[Mo(CO)_5CN]^-$ (ν(C≡N) 2099 cm^{-1}) [3c]. The influence of the coordination is also clearly reflected in the ^{95}Mo-NMR spectrum of both compounds in comparison with the cyanopentacarbonyl. The ^{95}Mo-NMR resonance is shifted to a lower field relative to the anion $[Mo(CO)_5(CN)]^-$ (**2**) (δ- 1882 ppm, at room temperature) [3a,c].

The strongest shift difference can be seen in the signal corresponding to the carbon atom of the bridging cyano group. The ^{13}C-NMR signal corresponding to the carbon atom of the bridging cyano group is shifted in **13** and **14** to a lower field ($[Mo(CO)_5CN]^-$ δ 149.2 ppm).

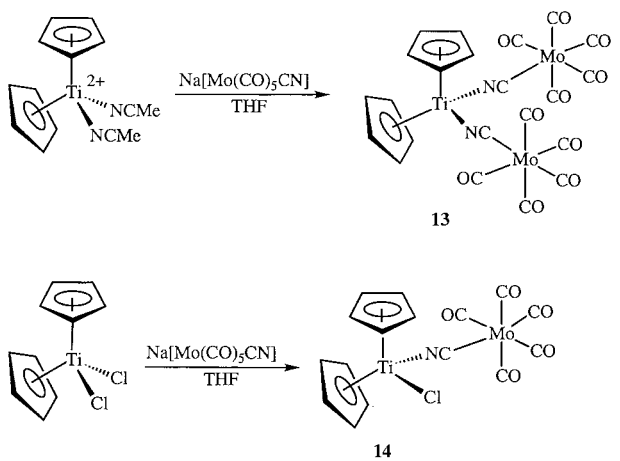

Scheme 2.

Table 2
Selected bond lengths (Å) and angles (°) for the complex cation $[Cp_2W\{-NC-Mo(CO)_5\}]^+$ **3**$^+$

Bond length			
W–C(31)	1.970(19)	W–N(1)	2.102(11)
Mo–C(1)	2.164(14)	Mo–C(41)	2.05(3)
Mo–C(51)	1.99(2)	Mo–C(61)	1.90(3)
Mo–C(71)	1.99(3)	Mo–C(81)	1.96(2)
N(1)–C(1)	1.124(15)		
Bond angles			
C(31)–W–N(1)	89.0(6)		
C(1)–N(1)–W	177.5(12)	N(1)–C(1)–Mo	173.6(14)
C(41)–Mo–C(1)	90.7(8)	C(51)–Mo–C(1)	92.6(6)
C(61)–Mo–C(1)	87.4(7)	C(71)–Mo–C(1)	86.4(7)
C(81)–Mo–C(1)	178.3(8)	C(51)–Mo–C(41)	88.0(11)
C(61)–Mo–C(41)	95.1(14)	C(71)–Mo–C(51)	88.1(9)
C(61)–Mo–C(51)	176.9(11)	C(61)–Mo–C(71)	88.8(12)
C(61)–Mo–C(81)	91.3(9)	C(81)–Mo–C(71)	92.6(9)
C(81)–Mo–C(51)	88.7(8)	C(81)–Mo–C(41)	90.4(11)
C(71)–Mo–C(41)	175.0(12)		

2.2. Crystallography

The X-ray diffraction study of complex $[Cp_2W(CO)\{-NC-Mo(CO)_5\}]BF_4$ (**3**) shows that its crystal structure is built up from an asymmetric unit composed of one complex cation $[Cp_2W\{-NC-Mo(CO)_5\}]^+$, **3**$^+$, one disordered BF_4^- anion, and one solvent molecule of diethyl ether with an occupancy factor of 0.5. Selected bond distances and angles are given in Table 2 for **3**$^+$. Standard deviations are slightly high, reflecting the thermal and positional disorder found for the carbonyl groups and the BF_4^- anion, respectively. However, the metric parameters listed have enough accuracy to characterise unequivocally the co-ordination sphere of both the metal centres. A PLUTON style diagram [15] showing the overall geometry of this binuclear complex with atomic notation scheme used is presented in Fig. 1.

The molybdenum and tungsten centres are linked by a cyanide bridge with Mo–C and W–N distances of 2.164(14) and 2.102(11) Å, respectively. Further, the W, N(1), C(1), and Mo atoms define an almost collinear arrangement giving rise to W–N(1)–C(1) and Mo–C(1)–N(1) angles of 177.5(12) and 173.6(14)°, respectively. Many examples of M–C≡N–M′ metal transition bridges, characterised by X-ray crystallography, are available from the literature. In fact, from a survey on the Cambridge Crystallography Data Base [16] 236 items were retrieved containing two metal transition centres connected by cyanide bridges in geometric arrangements ranging from the perfect linear to the strongly bent. The M–C≡N and C≡N–M′ bond angles are in the ranges of 180.0–136.7° and 180.0–113.7°, respectively. Among this large number of structures there are no examples of W–N≡C–Mo bridges. However, one complex with M–N≡C–Mo (M = Mn) bridges and three complexes with W–N≡C–M′ (M = W) bridges were retrieved. Table 3 lists the molecular dimensions of the cyanide bridges in these complexes together with their formulas, CSD refcodes and sources.

Complexes **16** and **18** contain only two tungsten centres bridged by a cyanide ligand, as described for the

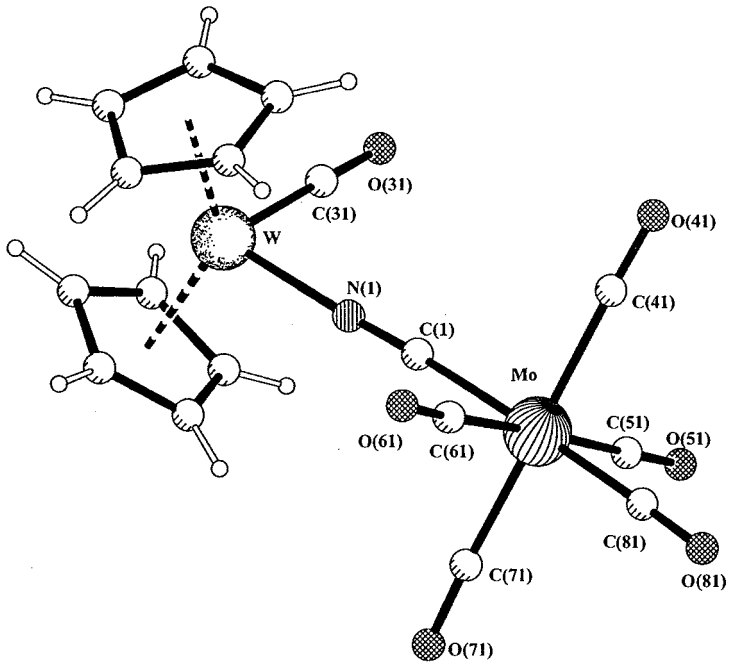

Fig. 1. A PLUTON view [15] of $[Cp_2W\{-NC-Mo(CO)_5\}]^+$ (**3**) showing the molecular geometry and the atomic notation scheme adopted. For clarity only the atomic notation for the quoted atoms in the text is included.

Table 3
Molecular dimensions of M–N≡C–M′ metal transition bridges related to the studied complex

CSD refcode	Bridge	Distances (Å)			Bond angles (°)		References
		W–N	Mo–C	N≡C	M–N≡C	N≡C–M′	
3	[M = W; M′ = Mo]	2.102(11)	2.164(14)	1.124(15)	177.5(12)	173.6(14)	This work
16 HAQVAW	[M = W; M′ = W]	2.127		1.166	170.6	174.3	[17]
17 GIMYOQ [a]		2.174		1.121	171.8	160.2	[18]
		2.217		1.158	168.3	159.7	
		2.151		1.175	163.5	166.7	
18 PIFFUF		2.190		1.148	172.8	175.7	[19]
19 BOCMEL [a]	[M = Mn; M′ = Mo]		2.156	1.161	175.2	148.4	[20]
			2.149	1.169	177.0	142.9	
			2.204	1.148	175.8	146.5	
			2.174	1.160	176.4	150.6	
			2.206	1.206	177.0	147.3	

HAQVAW, (μ_2-Cyano)-bis{hydrogen tris(3,5-dimethylpyrazolyl)borato}(η^2-phenylpropyne)(η^2-hexene)-bis(carbonyl-tungsten)tetrakis{3,5-bis-(trifluoromethyl)phenyl}borate. GIMYOQ, tris(μ_2-Cyano)tris(tricarbonylnitrosyltungsten). PIFFUF, Dicarbonyl(μ_2-carbonyl)-bis(η^5-cyclopentadienyl)-(μ_2-piperidylidenemethylene-C,C)-diiron (μ_2-cyano)decacarbonylditungsten. BOCMEL, catena(decakis(μ_2-Cyano)-diaquatridecacyanohexakis(2,13-dimethyl-3,6,9,12,18-pentaazabicyclo[12.3.1]octadeca-1(18),2,12,14,16-pentaene)trimanganesetrimolybdenum hydrate).

[a] Complexes **17** and **19** contain three W–N≡C–W and five Mn–N≡C–Mo bridges, respectively.

complex studied, and the W–C≡N and C≡N–W bond angles take values close to 180°, indicating that the cyanide bridge is only slightly bent. In complex **17**, three $W(CO)_4$ units are connected by three cyanide bridges, leading to a cyclic structure with W–C ≡ N angles of 166.7, 160.2 and 159.7° and W–N ≡ C angles of 171.8, 168.0 and 163.5°. In the crystal of **19**, the supramolecular assembly contains units [MnLCO] (L = catena-{decakis(μ_2-cyano)-diaquatridecacyanohexakis-(2,13-dimethyl3,6,9,12,18-penta-azabicyclo(12.3.1)octadeca-1(18),2,12,14,16-pentaene}-tri-manganese-trimolybdenum hydrate) and $Mo(NC)_n$ ($n = 7$, 8), where cyanide groups bridge the two metal centres in a complicated arrangement. The Mo–C ≡ N angles are near 180°, while the C ≡ N–Mn angles show bending of the cyanide bridges at the nitrogen centres, probably because of crystal packing.

Moreover, the N ≡ C bond distance of 1.124(15) Å in **3** is slightly shorter than that found for the free gaseous HCN of 1.156 Å [21] indicating undoubtedly that in **3** the cyanide bridge retains its triple bond character. This result is consistent with the IR spectrum, which shows a ν(C ≡ N) vibration at 2116 cm^{-1} characteristic of a cyanide bridge (see above). Further, the N–C distance in **3** is one of the shortest values reported in Table 3 for C ≡ N bonds.

The co-ordination geometry around the W centre, comprising the centroids of two η^5-C_5H_5 rings, one carbonyl ligand, and the NC moiety, can be described as a distorted pseudo-tetrahedron, while the cyanide bridge and five carbonyl groups surround the molybdenum centre in a distorted octahedral co-ordination environment. The tungsten is 1.988 and 1.987 Å away from the centroids of the Cp rings, leading to a centroid–W–centroid angle of 137.2°. The angle CN–W–CO is 89.0(6)°. Similar geometric arrangements, with comparable structural parameters, were found for a few related monuclear W(IV) complexes $[Cp_2W(NCMe)(Et)]^+$ (**20**), [22] and $[Cp_2W(NCMe)_2]^{2+}$ (**17**) [23]. Moreover, the W–N distances (2.113 Å in **16** and an average value of 2.094 Å in **17**) and N ≡ C (1.120 Å in **16** and an average value of 1.136 Å in **17**) are also similar to those found for $[Cp_2W(CO)\{-NC-Mo(CO)_5\}]BF_4$ (**3**). This comparison indicates that the structure of the $Cp_2W(IV)CO(N \equiv C)$ fragment is not greatly disturbed by the presence of the second fragment, $Mo(CO)_5$. Therefore, the metallocene fragment of the complex studied presents molecular dimensions typical of $[Cp_2MLL']$ systems.

2.3. DFT calculations

The DFT calculations [10] were performed using the ADF program [24] on selected complexes (see Section 3), starting from complex **3**, $[Cp_2W(CO)\{-NC-Mo(CO)_5\}]^+$, as its structure was experimentally determined and therefore provides a good way to check the quality of the results. Full geometry optimisations without any symmetry constraints were carried out in all cases. The relevant distances and angles for complex **3** in the optimised geometry are shown in Scheme 3 (a), while those observed in the X-ray structure can be seen in Scheme 3 (b). There is a good agreement between the experimental (Table 2) and the calculated structures, both for angles and bond lengths.

The structures of complexes $[Cp_2Mo(CO)\{-NC-Cr(CO)_5\}]^+$ (**4**), $[IndCpMo(CO)\{-NC-Cr(CO)_5\}]^+$ (**5**), $[Cp_2TiCl\{-NC-Mo(CO)_5\}]^+$ (**14**), and $[IndCpMo(CO)(NCMe)]^{2+}$ (**20**) were also fully optimised under the same conditions, and the final geometries are depicted in Scheme 4, along with the relevant geometrical parameters.

This group of complexes was selected to analyse the effect of several parameters on both the electronic spectra and electrochemical results (see the following sections). The CN distances are very similar in all the binuclear complexes, but shorter in the mononuclear one where it belongs to a nitrile. In the binuclear species, metal–CN back donation is expected, though not with M–NC, as isonitriles are π-acceptors, but nitriles are π-donors. This effect should be responsible for the lengthening of the CN bond. Note that in the two mixed ring complexes, **5** and **20**, the indenyl adopts the preferred conformation, observed before now in similar complexes, [6,25] where the benzene does not lie *cis* or *trans* relative to the two ligands CO and NCR, but halfway between these positions. The L–M–L′ angles in the bisector plane of the rings of the metallocene also adopt the standard values, between 86 and 88° for Mo, and W, but becoming wider (95°) in the Ti derivative, as expected from their respective d^2 and d^0 electron count [26].

The nature of the frontier orbitals of complexes $[Cp_2W(CO)\{-NC-Mo(CO)_5\}]^+$ (**3**), $[Cp_2Mo(CO)\{-NC-Cr(CO)_5\}]^+$ (**4**), $[IndCpMo(CO)\{-NC-Cr(CO)_5\}]^+$ (**5**), $[Cp_2TiCl\{-NC-Mo(CO)_5\}]^+$ (**14**), and $[IndCpMo(CO)(NCMe)]^{2+}$ (**20**) was investigated. The composition of the HOMO and LUMO of the five complexes, as well as their relative energies are summarised in Table 4 and will be used to discuss the electrochemical results below.

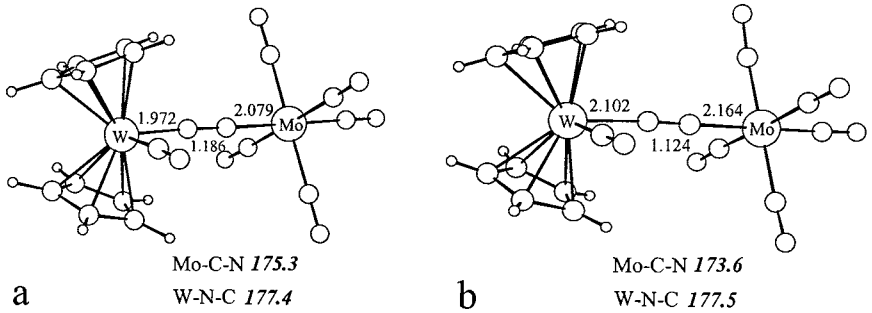

Scheme 3.

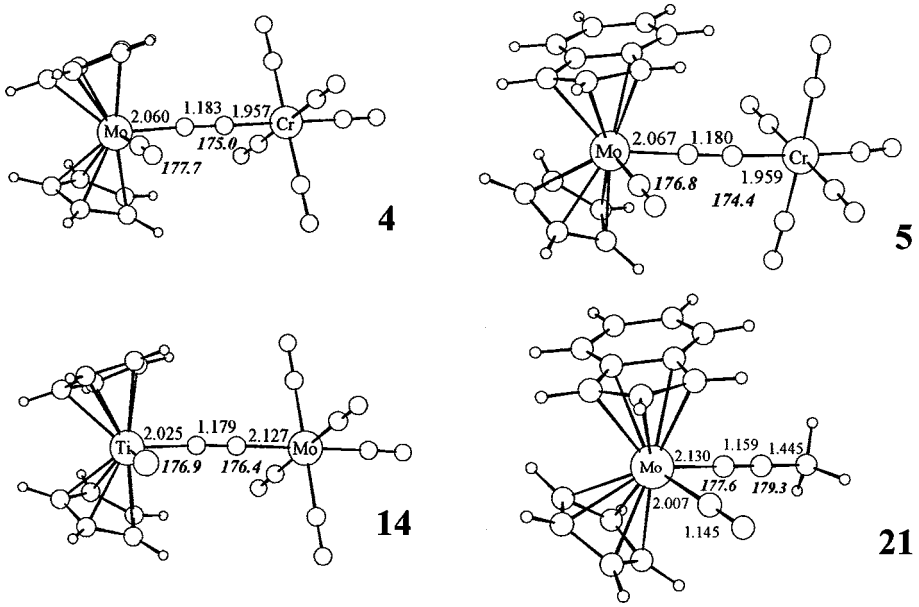

Scheme 4.

Table 4
The composition (%) and energies (kJ mol^{-1}) of the HOMO and LUMO of the [Cp(Ring)MX{–CN–M′(CO)$_5$}] complexes (Ring = Cp, Ind) (DFT calculations)

	Complex									
	(**3**) W [a]–Mo		(**4**) Mo [a]–Cr		(**5**) Mo [a]–Cr		(**14**) Ti [a]–Mo		(**20**) Mo [a]	
	HOMO	LUMO	HOMO	LUMO	HOMO	LUMO	HOMO	LUMO	HOMO	LUMO
Energy	−777.38	−744.61	−759.35	−721.07	−752.41	−716.28	−525.18	−383.28	−1226.04	−1004.94
M [a]	2.2	26.5	2.5	33.9	3.4	33.6	0.0	70.3	56.8	36.3
M′	56.7	1.2	56.3	1.3	53.8	1.1	55.3	2.0	–	–
Rings	1.7	47.1	1.2	46.8	2.5	48.8	17.2	8.7	20.2	50.4
CO(M [a])/Cl	1.5	28.1	0.8	18.1	1.0	14.7	0.0	9.4	10.9	12.8
N	8.2	0.2	8.0	0.2	8.0	0.7	7.8	0.5	0.8	1.2
C	0.5	0.0	0.2	0.1	0.3	0.2	0.0	5.7	6.2	0.2
(CO)$_5$	28.2	0.7	29.3	0.7	28.7	0.6	17.9	1.0	1.3	–

[a] Metal in metallocene.

Time dependent DFT calculations (TD-DFT) [27] were used to determine the excitation energies for the electronic transitions in the selected complexes, although the more interesting one is complex **14** [Cp$_2$TiCl{–NC–Mo(CO)$_5$}]$^+$, containing a 16 electron centre (Ti), in opposition to Mo and W 18 electron centres. A metal-to-metal charge-transfer band is therefore expected. The results will be shown and discussed below (Section 2.5).

2.4. Electrochemical studies

Relevant electrochemical data for the complexes in MeCN or CH_2Cl_2 (containing 0.1 M tetrabutylammonium hexafluorophosphate) are listed in Table 5. All voltammograms were started at 0 V in anodic sweep and the potentials calibrated with internal ferrocene standard (see Section 3). Data for [Cp$_2$W(CO)(NCMe)][BF$_4$]$_2$ (**7**), [CpCp′M(L)(NCMe)][BF$_4$]$_2$ (Cp′ = Cp, Ind; L = CO, MeCN) and Na[M′(CO)$_5$CN] (M′ = Mo (**2**), Cr (**11**)) are included for comparison.

The cyclic voltammogram (CV) of complex [Cp$_2$W(CO){NC–Mo(CO)$_5$}]BF$_4$ (**3**) in MeCN shows an irreversible oxidation at 1.11 V versus SSC and an irreversible reduction at −0.82 V. Both the related complex [Cp$_2$W(CO)(NCMe)][BF$_4$]$_2$ (**7**), and the organometallic fragment [Mo(CO)$_5$CN]$^-$ (**2**) present irreversible waves in their CVs: the former presents irreversible reductions and the latter an irreversible oxidation. A more interesting situation is found in the voltammogram of [Cp$_2$Mo(CO){NC–Cr(CO)$_5$}]BF$_4$ (**4**), which exhibits two not well-resolved electrochemically quasi-reversible oxidations and one irreversible reduction. The lack of reversible reductive behaviour is expected as free [Cr(CO)$_5$CN]$^-$ (**11**) is not reduced within the solvent limits and no reversible reductive electrochemistry has ever been observed for Cp$_2$Mo(IV) complexes. On the contrary, they may undergo reversible oxidation to the Cp$_2$Mo(V) oxidation state, [28] and free [Cr(CO)$_5$CN]$^-$ (**11**) presents a reversible wave at 0.69 V (vs. SSC) in the MeCN solvent. The HOMO of complex **4** has a localisation of 56.3% in Cr and 85.6% in the Cr(CO)$_5$ fragment, allowing us to assign the wave at $E_{pa} = 0.98$ V to the oxidation of the Cr centre in **4**. This is in keeping with the fact that the [Cp$_2$Mo(CO)]$^{2+}$ (**6**) fragment withdraws the electronic charge from [Cr(CO)$_5$CN]$^-$ (**11**). In complex **4**, where Cr exhibits an almost octahedral environment, the three highest occupied orbitals have energies within a close window (−760.4, −772.4, −792.4 kJ mol^{-1}), two of them having close energies, and the third one being more stable. The contribution of Cr(CO)$_5$ is 85.6, 84.6, and 98.2%, respectively. The next orbital, with a strong contribution from Mo, has energy of 131 kJ mol^{-1} lower, indicating that all the oxidation processes should be related to Cr. However, in order to have more reliable information on the nature of the HOMOs, calculations on the paramagnetic oxidised and dioxidised species were performed. The HOMO was in all possibilities mainly localised on Cr, as expected. The peak at $E_{pa} = 1.12$ V can thus be assigned to a second oxidation of the Cr centre in **4** as represented in Scheme 5. After the second oxidation process, the diradical paramagnetic species is more stable, according to the calculations, than the alternative diamagnetic one. As expected, the irreversible process at −0.57 V is assigned to the reduction of Mo as a result of the localisation of the LUMO in the Mo (33.9%) or in the Cp$_2$Mo fragment (80.7%).

The CV of [IndCpMo(CO){NC–Cr(CO)$_5$}]BF$_4$ (**5**) in MeCN presents a quasi-reversible oxidation wave (oxidation of Cr, see Table 5) a reduction at −0.38V with a distorted back wave at −0.22 V (Fig. 2). As we have shown before [6a] the mixed-ring metallocene analogues IndCpMo(IV) have a richer electrochemistry than their

Table 5
Cyclic voltammetry data (recorded in NCMe)

Compound	E_{pa} (V) [a]	E_{pc} (V) [b]	Comment
2 $[Mo(CO)_5CN]^-$ [c]	0.85	–	–
3 $[Cp_2W(CO)\{NC–Mo(CO)_5\}]BF_4$	1.11		
	–	−0.82	–
4 $[Cp_2Mo(CO)\{NC–Cr(CO)_5\}]BF_4$	0.98	0.88	qr
	1.12	1.00	qr
	–	−0.57	–
5 $[IndCpMo(CO)\{–NC–Cr(CO)_5\}]BF_4$	0.99	0.86	qr
	−0.22	−0.38	irr
7 $[Cp_2W(CO)(NCMe)]^{2+}$	–	−0.27	–
	–	−0.63	–
8 $[Cp_2Mo(CO)(NCMe)]^{2+}$	−0.24	−0.30	irr
10 $[Cp_2Mo(NCMe)_2]^{2+}$	−1.00	−0.78	irr
	−0.42	−1.05	qr
22 $[IndCpMo(NCMe)_2]^{2+}$	−0.51	−0.56	irr
	−0.71	−0.72	irr
	–	−0.88	–
11 $[(CO)_5CrCN]^-$ [d]	0.73	0.65	rev
13 $Cp_2Ti\{NC–Mo(CO)_5\}_2$	1.24	–	–
	−0.05	−0.01	qr
	−0.25	−0.32	rev
14 $Cp_2TiCl\{–NC–Mo(CO)_5\}$ [e]	1.21	–	–
	−0.56	−0.74	irr
	−0.99	−1.15	qr

[a] E_{pa} — anodic sweep (peak potentials, V).
[b] E_{pc} — cathodic sweep (peak potentials, V).
[c] See also Ref. [3b].
[d] See also Refs. [3b,12].
[e] Recorded in CH_2Cl_2.

parent $Cp_2Mo(IV)$ species, namely in reduction. The dications $[IndCpMoL_2][BF_4]_2$ (L = bipy, $^tBu_2$bipy, dppe, $P(OMe)_3$, etc.) undergo two consecutive reductions accompanied by indenyl-slippage from (η^5-Ind)CpM(IV) → (η^3-Ind)CpM(II) [6]. This kind of process is certainly the one observed at $E_{pc} = -0.38$ and $E_{pa} = -0.22$ V versus SSC, and is in agreement with the composition of the LUMO, which is mainly located on the metallocene fragment. The two features at ca. −0.7 and −1.1 V remain unidentified but are probably related to the species either derived from further redox induced indenyl slippage steps or rearrangement/decomposition of the species formed at −0.38 V. This is not unexpected as nitrile complexes like $[IndCpMo(NCMe)X]^{n+}$ (X = Br, $n = 1$; X = NCMe; $n = 2$) do not undergo clean chemical or electrochemical reduction, and therefore, we made no further efforts to pursue with the clarification of the voltammogram in the negative potential region [6c,d].

The value of the peak potentials for the oxidation is very similar to those reported for **4**, and, therefore, can be assigned to the oxidation of the Cr centre, in agreement with the HOMO composition (Table 4). In THF this oxidation becomes reversible at $E_{pa} = 1.16$ V/$E_{pc} = 1.20$ versus SSC but the reduction becomes totally irreversible at $E_{pc} = -0.3$ V versus SSC. Considering that the $Cr(CO)_5CN$–MoCpInd linkage is electronically similar to a RCN–Mo MoCpInd linkage, several nitrile

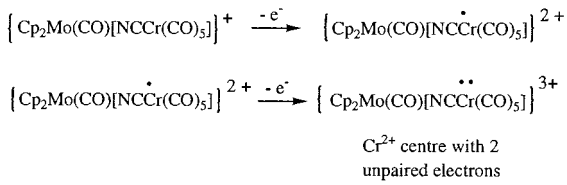

Scheme 5.

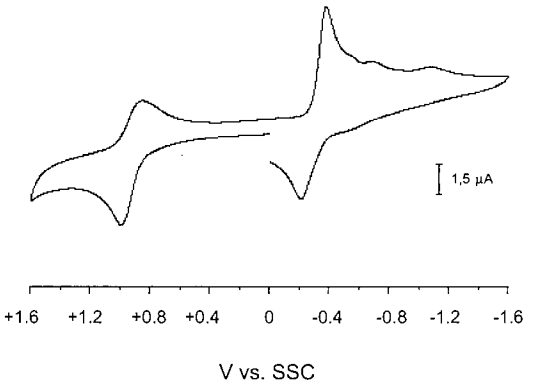

Fig. 2. Cyclic Voltammogram of $[IndCpMo(CO)\{–NC–Cr(CO)_5\}]BF_4$ (**5**) at 298K in MeCN/0.1M $[Bu_4N][PF_6]$ ($V = 200$ mV s^{-1}).

Table 6
Electronic spectral data for various mononuclear and cyanide-bridged polynuclear complexes, in MeCN

Compound	ν_{max} (nm) (ε, $cm^{-1}\,mol^{-1}\,dm^3$)
2 $Na[Mo(CO)_5CN]$	357 (1980); 325 (1570); 254 (32800); 236 (31300)
3 $[Cp_2W(CO)\{-NC-Mo(CO)_5\}]BF_4$	sh 350 (3140); sh 318 (5010); 235 (45200)
4 $[Cp_2Mo(CO)\{-NC-Cr(CO)_5\}]BF_4$	sh 336 (4200); 227 (37800)
5 $[IndCpMo(CO)\{-NC-Cr(CO)_5\}]BF_4$	sh 517 (425); 340 (4620); 228 (46300)
7 $[Cp_2W(CO)(NCMe)][BF_4]_2$	sh 420 (130); 358 (210); sh 321 (250); sh 240 (5410)
11 $Na[Cr(CO)_5CN]$	341 (2200); 247.5 (32600); sh 230 (30500)
12 $[Cp_2Ti(NCMe)_2][PF_6]_2$	sh 490 (150); sh 340 (2400); 246 (23800)
13 $Cp_2Ti\{-NC-Mo(CO)_5\}_2$	545 (5800); 342 (8800); sh 254 (96200); 236 (115800)
14 $Cp_2TiCl\{-NC-Mo(CO)_5\}$	480 (3610); sh 351 (6350); 236 (67200)
20 $[IndCpMo(CO)(NCMe)][BF_4]_2$	456.5 (420); sh 352 (1430); sh 284 (6800); sh 258 (13900), 237 (17800)
21 $[IndCpMo(NCMe)_2][BF_4]_2$	537 (230); 430 (250); sh 335 (1320); sh 280 (2400); 246 (23760)

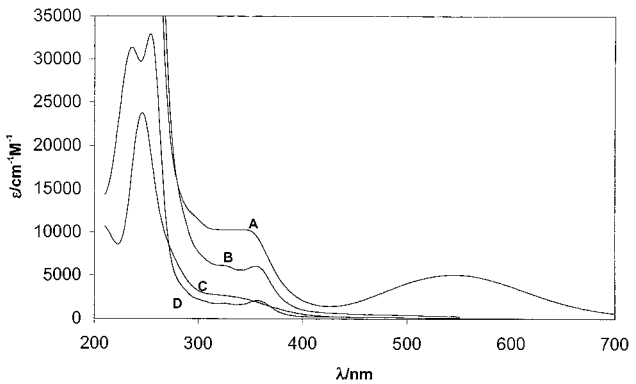

Fig. 3. Absorption spectra of compound $Cp_2Ti\{NC-Mo(CO)_5\}_2$ (**13**) (A), and model compounds $Na[Mo(CO_5)CN]$ (**2**) (D) and $[Cp_2Ti(NCMe)_2][PF_6]_2$ (**12**) (C) in CH_3CN; $B = 2 \times D + C$.

analogues of complexes **1**–**5** were also studied. The cyclic voltammograms of the dications $[Cp_2W(CO)(NCMe)][BF_4]_2$ (**7**) and $[Cp_2Mo(CO)(NCMe)][BF_4]_2$ (**8**) and $[Cp_2Mo(NCMe)_2][BF_4]_2$ (**10**) only show electrochemical activity in the range from 0 to -0.9 V corresponding to the irreversible reductions. Complexes with an indenyl fragment IndCpM, e.g. $[IndCpMo(NCMe)_2][BF_4]_2$ (**21**) (Table 5) also show irreversible reduction waves. The energies of HOMO and LUMO calculated for $[IndCpMo(CO)(NCMe)]^{2+}$ (**20**) are completely different from those of the binuclear species, showing that even if the $Cr(CO)_5CN$ fragment does not significantly change the molecular structure, it significantly modifies the electronic structure.

The electrochemistry of the Cp_2Ti derivatives $Cp_2TiCl\{NC-Mo(CO)_5\}$ (**14**) and $Cp_2Ti\{NC-Mo(CO)_5\}_2$ (**13**) is irreversible in the oxidation segment. The composition of the HOMO of **14** would suggest the oxidation of the Mo centre, and the irreversible behaviour is very similar to the one observed in the uncoordinated $[Mo(CO)_5(CN)]^-$ (**2**). The negative potential region of complex **13** shows two redox pairs of closely spaced reductions, Table 5. These waves are associated with Ti(IV) reduction to the putative $[Cp_2Ti\{NC-Mo(CO)_5\}_2]^{2-}$, isoelectronic with $[Cp_2Mo\{NC-Mo(CO)_5\}_2]$, and agrees with the LUMO composition (calculated for **14**).

2.5. Electronic spectra

Absorption spectral data for the cyanide-bridged polynuclear compounds as well as for some mononuclear model compounds are reported in Table 6. With the exception of Ti–Mo compounds **13** and **14**, there are no prominent features in the visible region, the bands presenting more or less the pattern of the mononuclear moieties with little red-shifts compared with them. The Ti–Mo compounds, however, present new bands in the visible region ($\varepsilon_{480} = 3610\ cm^{-1}\,M^{-1}$ for compound **14**; $\varepsilon_{545} = 5800\ cm^{-1}\,M^{-1}$ for compound **13**, Fig. 3) that can be assigned as metal-to-metal charge transfer transitions.

Fig. 3 shows this band in the absorption spectrum of compound **13** which is clearly not present in the mononuclear compounds $Na[Mo(CO_5)CN]$ (**2**) and $[Cp_2Ti(NCMe)_2][PF_6]_2$ (**12**). As referred above, Ti(IV) in compounds **13** and **14** are 16 electron centres while Mo(IV) are 18 electron centres; the observed new bands are therefore $Mo \rightarrow Ti$ charge transfer transitions; which cannot be observed in the W–Mo compounds (both 18 electron centres). The high intensity of the $Mo \rightarrow Ti$ charge transfer bands appears to be normal for cyanide-bridged polynuclear complexes; ε values in the order of magnitude of 10^3 are commonly observed [1i,12,29a,b].

TD-DFT calculations (Table 7) allow the calculation of excitation energies and the corresponding oscillator strengths. For complex $Cp_2TiCl\{NC-Mo(CO)_5\}$ (**14**), there are two bands at 473 and 442 nm with oscillator strengths of 0.072 and 0.0463, respectively, which may account for the band observed in the UV–vis spectrum at 480 nm. The excitation at 473 nm consists of a HOMO to LUMO + 1 (92%), while the other one consists of a HOMO to LUMO + 2 (94%). The compositions of the HOMO and LUMO are given in Table 4, the HOMO being associated with the $Mo(CO)_5$ fragment (73.2%) and the CN bridge (7.8%). The LUMO + 1 and LUMO + 2 orbitals are essentially located in the CpTiCl fragment (92.6 and 95.9%, respectively). This confirms that the observed transition can be assigned to a $Mo \rightarrow Ti$ charge transfer.

Table 7
Calculated (TD-DFT) and experimental excitation energies (visible) and their assignments

	Energy (nm)	Oscillator strength	MO transition	Cont.	%
Calculated	473.03	0.07204	HOMO → LUMO + 1	71a → 73a	92
Calculated	442.06	0.04629	HOMO → LUMO + 2	71a → 74a	94
Experiment	480	0.056197			

Acetonitrile solutions of **13** and **14** change colour very easily under UV–vis light while they remain unchanged if kept in the dark (O_2 does not interfere significantly in this process as essentially the same results were observed in aerated and deaerated solutions). Irradiation at 546 nm was carried out to check for photochemical reactions arising from the Mo → Ti charge transfer excited state. However, no spectral changes were observed upon 1-h irradiation, indicating that the decomposition reactions observed on light exposure arise from higher excited states.

3. Experimental

3.1. Materials and procedures

All the experiments were carried out under N_2 atmosphere by Schlenk techniques. Diethyl ether, THF and pentane were dried by distillation from Na/benzophenone. Acetonitrile was dried over P_2O_5 and distilled after refluxing for several hours over P_2O_5. Dichloromethane was distilled from P_2O_5. Acetone was distilled over K_2CO_3 and kept over 4 Å molecular sieves.

Microanalyses were performed by Z. Tavares in our laboratories (ITQB). ^{1}H-NMR spectra were obtained with a Bruker CXP 300 spectrometer. IR spectra were recorded on a Unican Mattson Mod 7000 FTIR spectrophotometer using KBr pellets and/or in solution.

The ^{95}Mo- and ^{13}C-NMR spectra were obtained in a Bruker ARX400 instrument with a 5 mm multinuclear probe. The ^{95}Mo spectra were performed with a zg pulse program, with the probe tuned to 26.08 MHz and a pre-acquisition delay between 50 and 200 ms (to reduce the probe ringing). The p/2 pulse was found to be 30 ms. The acquisition time was 0.1 s with a resolution of 5 Hz.

The electrochemical instrumentation consisted of a BAS CV-50W-1000 Voltammetric Analyser connected to BAS/Windows data acquisition software.

All the electrochemical experiments were run under argon at room temperature (r.t.). Tetrabutylammonium hexafluorophosphate (Aldrich) recrystallised from ethanol was used as the supporting electrolyte. Cyclic voltammetry experiments were performed in a glass cell MF-1082 from BAS in a C-2 cell enclosed in a Faraday cage. The reference electrode was SSC (MF-2063 from BAS), and its potential is approximately −44 mV relative to a SCE. The reference electrode was calibrated with a solution of ferrocene (1 mM) to obtain a potential in agreement with the literature value [30].

The auxiliary electrode was a 7.5 cm platinum wire (MW-1032 from BAS) with a gold-plated connector. The working electrode was a Platinum disk (MF-2013 from BAS) with ca. 0.022 cm^2 sealed in Kel-F plastic. Between each CV scan the working electrode was electro-cleaned, polished on Diamond 1 μM and Alumina cleaned with water–methanol and sonicated before use, according to standard procedures. Solvents were dried as previously described. The electrochemical experiments on each complex were followed by the addition of ferrocene to the solution, and a new cyclic voltammogram was recorded. The electrochemical behaviour of the complexes did not seem to be affected by the presence of ferrocene and vice versa.

Electronic Spectra and photochemical studies: all the solutions were prepared and handled in the dark. Acetonitrile was dried over CaH_2 and distilled before use. Electronic absorption spectra were run on a Perkin–Elmer lambda 6 UV–vis spectrophotometer. Irradiation experiments were carried out in PTI instrumentation, using a medium pressure Hg lamp (HBO 100 W) mounted in a lamphouse (Model A1010) connected to a LPS-220 Lamp Arc Supply. Light of 546 nm was isolated from the medium pressure Hg lamp by means of an interference filter (P/N 56460 Allied Electro Optics (Italy); $\nu_{max} = 546.1$ nm).

$Na[M(CO)_5(CN)]$ (M = Mo, Cr) [31], $[Cp_2W(CO)_2][BF_4]_2$ [6], $IndCpMoCl_2$ [6a], $[CpCp'Mo(CO)_2][BF_4]_2$ (Cp′ = Cp, Ind) [6a], $[IndCpMo(NCMe)_2][BF_4]_2$ [6a], Cp_2TiCl_2 [14], $[Cp_2Ti(NCMe)_2][PF_6]_2$ [13] $CpMo(\eta^3\text{-}C_3H_5)(CO)_2$ [6a], were prepared as described previously.

3.2. Preparation of $[Cp_2W(CO)\{-NC-Mo(CO)_5\}]BF_4$ (3)

A suspension of $[Cp_2W(CO)_2][BF_4]_2$ (0.20 g, 0.37 mmol) in CH_2Cl_2 (20 ml) was treated with a solution of $Na[Mo(CO)_5(CN)]$ (0.12 g, 0.42 mmol) in THF (5 ml). After 1 h the resulting yellow solution was filtered, washed with ether and recrystallised from a mixture of acetone–CH_2Cl_2–ether. Yield: 0.21 g (82%). Anal. Found: C, 30.00; H, 1.33; N, 1.69. Calc. for $C_{17}H_{10}NO_6BF_4MoW$: C, 29.56; H, 1.46; N, 2.03%. IR (KBr, cm^{-1}): ν 3123m, 3090m, 2116m, 2060s, 2045s,

2006w, 1989w, 1925vs, 1903vs, 1435m, 1413m, 1085s, 1068s, 1037s, 873m, 691s, 607m, 590s. IR (MeCN, cm^{-1}): ν 2120m, 2062s, 2050s, 1946vs. ^{1}H-NMR (CD_3COCD_3, 300 MHz, r.t., δ ppm): 6.56 (s, 10H, Cp). ^{13}C-NMR (CD_3CN, 300 MHz, r.t., δ ppm): 216.1, 209.0, 204.9 (CO); 194.5 (CN); 96.4 (Cp).

3.3. Preparation of $[Cp_2Mo(CO)\{-NC-Cr(CO)_5\}]BF_4$ (4)

A suspension of $[Cp_2Mo(CO)_2][BF_4]_2$ (0.34 g, 0.75 mmol) in CH_2Cl_2 (20 ml) was treated with a solution of $Na[Cr(CO)_5CN]$ (0.18 g, 0.75 mmol) in THF (5 ml). After 5 h the resulting yellow solution was filtered, washed with ether and recrystallised from acetone–ether. Yield: 0.29 g (70%). Anal. Found: C, 37.09; H, 2.08; N, 2.48. Calc. for $C_{17}H_{10}NO_6BF_4CrMo$: C, 36.53; H, 1.80; N, 2.51%. IR (KBr, cm^{-1}): ν 3121s, 2118s, 2056vs, 1915vs, 1441m, 1416m, 1084vs, 854m, 657s. IR (MeCN, cm^{-1}): ν 2120m, 2072s, 2058s, 1942vs. ^{1}H-NMR (CD_3COCD_3, 300 MHz, r.t., δ ppm): 6.63 (s, 10H, Cp). ^{13}C-NMR (CD_3CN, 300 MHz, r.t., δ ppm): 219.9, 216.7, 212.1 (CO); 194.9 (CN); 100.9(Cp).

3.4. Preparation of $[IndCpMo(CO)\{-NC-Cr(CO)_5\}]BF_4$ (5)

A suspension of $[IndCpMo(CO)_2]$ $[BF_4]_2$ (0.33 g, 0.65 mmol) in CH_2Cl_2 (20 ml) was treated with a solution of $Na[Cr(CO)_5CN]$ (0.16 g, 0.65 mmol) in THF (5 ml). After 2 h the resulting solution was evaporated. The brown powder was efficiently extracted with dichloromethane, evaporated and washed with ether. Yield: 0.28 g (70%). Anal. Found: C, 41.07; H, 1.94; N, 2.04. Calc. for $C_{21}H_{12}NO_6BF_4CrMo$: C, 41.41; H, 1.99; N, 2.30%. IR (KBr, cm^{-1}): ν 3117m, 2116s, 2054s, 1911vs, 1541m, 1447m, 1084vs, 860m, 764m, 658vs, 550m. IR (MeCN, cm^{-1}): ν 2118m, 2068s, 2058s, 1942vs. ^{1}H-NMR (CD_3CN, 300 MHz, r.t., δ ppm): 7.79–7.31 (c, 4H, H^{5-8}); 6.11 (s (alarg), 2H, $H^{1/3}$); 5.72 (t (alarg), 1H, H^2); 5.68 (s, 5H, Cp). ^{13}C-NMR (CD_3CN, r.t., δ ppm): 219.8, 216.7, 213.8 (CO); 192.5 (CN); 136.1, 135.2, 128.4, 128.1 (Ind); 102.0 (Cp); 90.5, 90.1, 87.3 (Ind).

3.5. Preparation of $Cp_2Ti\{-NC-Mo(CO)_5\}_2$ (13)

A suspension of $[Cp_2Ti(NCMe)_2][PF_6]_2$ (0.30 g, 0.54 mmol) in MeCN (25 ml) was treated with $Na[Mo(CO)_5CN]$ (0.31 g, 1.10 mmol). After 1 h the resulting solution was filtered, evaporated to dryness, washed with ether and recrystallised from CH_2Cl_2–ether. Yield: 0.25 g (80%). Anal. Found: C, 37.72; H, 1.25; N, 4.00. Calc. for $C_{22}H_{10}N_2O_{10}MoTi$: C, 37.64; H, 1.44; N, 3.66%. IR (KBr, cm^{-1}): ν 3125m, 2104s, 2049vs, 2029vs, 1993s, 1931vs, 1915vs, 1905vs, 1441m, 1259m, 1016m, 933m, 831vs, 677m, 660s, 604m, 588vs 546m. IR (NCMe, cm^{-1}): ν 2104m, 2050s, 1940vs. ^{1}H-NMR (CD_3COCD_3, 300 MHz, r.t., δ ppm): 6.92 (s, 10H, Cp). ^{13}C-NMR (CD_2Cl_2, 300 MHz, r.t., δ ppm): 208.5, 203.9 (CO); 193.7 (CN); 119.1 (Cp).

3.6. Preparation of $Cp_2TiCl\{-NC-Mo(CO)_5\}$ (14)

A solution of Cp_2TiCl_2 (0.20 g, 0.80 mmol) in THF (20 ml) was treated with $Na[Mo(CO)_5CN]$ (0.23 g, 0.80 mmol). After 90 min the resulting solution was reduced to dryness, and the residue was extracted with dichloromethane. Concentration of the dark red solution gave a powder. Yield: 0.33 g (88%). Anal. Found: C, 40.85; H, 2.04; N, 3.14. Calc. for $C_{16}H_{10}ClNO_5MoTi$: C, 40.41; H, 2.12; N, 2.95%. IR (KBr, cm^{-1}): ν 3105m, 2110m, 2052m, 1984m, 1937vs, 1439s, 1400m, 1248m, 1016s, 943m, 818vs, 588s. IR (MeCN, cm^{-1}): ν 2106m, 2048s, 1946vs. ^{1}H-NMR (CD_3COCD_3, 300 MHz, r.t., δ ppm): 6.79 (s, 10H, Cp). ^{13}C-NMR (CD_2Cl_2, 300 MHz, r.t., δ ppm): 204.4, 200.5 (CO); 182.8 (CN); 119.5 (Cp).

3.7. X-ray crystallography

Crystal data for **3**: $C_{18}H_{15}BF_4MoNO_{7.5}W$, $M_r = 730.91$, orthorhombic, space group *Pbca*, $a = 9.725(13)$, $b = 30.582(34)$, $c = 18.127(25)$ Å, $U = 5391.2(12)$ Å^3, $Z = 8$, $\rho_{calc} = 1.801$ mg m^{-3}, μ (Mo-Kα) = 4.790 mm^{-1}, 3447 reflections were collected. Final indices $R_1 = 0.0629$ and $wR_2 = 0.1904$ for 2539 reflections with $I > 2\sigma(I)$ and $R_1 = 0.0815$ and $wR_2 = 0.2128$ for all data.

X-ray data were collected at r.t. on a MAR research plate system using graphite Mo-Kα radiation (ν = 0.71073 Å) at the Reading University. The crystals were positioned at 70 mm from the image plate. Ninety-five frames were taken at 2° intervals using a counting time of 5 min. Data analysis was performed with the XDS program [32]. Intensities were corrected empirically for absorption effects, using a DIFABS version modified for image plate geometry [33].

The structure was solved by direct methods and by subsequent difference Fourier syntheses and refined by full-matrix least-squares on F^2 using the SHELX-97 system programs [34]. After all the positions of the non-hydrogen atoms were found it was clear from the Fourier difference maps that a molecule of the diethyl ether solvate was present in the asymmetric unit. The occupancy factor of this solvent molecule was set of the order of 0.50 to give reasonable isotropic thermal parameters and low R values. The hydrogen atoms on the carbon atoms were included in the calculated positions and the given thermal parameters were 1.2 times equivalent to those of the atom to which they were attached. The BF_4^- anion was disordered. Two sets of tetrahedral fluorine atoms were found and refined with occupancy factors x and $1 - x$, with x being refined to

0.46(2). Further, the dimensions of the BF_4^- anion as well as the diethyl ether were constrained during the refinement, using the DFIX instruction. All the non-hydrogen atoms of the complex cation $[Cp_2W\{-NC-Mo(CO)_5\}]^+$ and the boron atom were refined with anisotropic thermal displacements. The carbon atoms of the diethyl ether molecule were refined with individual isotropic temperature factors, while for the fluorine atoms a group isotropic thermal factor was included.

The analysis of anisotropic thermal parameters of the carbonyl ligands of the $Mo(CO)_5$ fragment indicates that they were presumably affected by some thermal and/or positional disorder. Then a trial model containing two alternative sites of each carbonyl ligand was considered. However, the refinement of this model was computationally unstable and afforded an unreasonable chemical structure.

The final difference Fourier Map calculated for complex **1** showed a residual electronic density in the range of 2.04 to -1.09 e $Å^{-3}$. However, the highest positive peak is within 0.06 Å of the tungsten atom while the largest hole was situated at 0.76 Å from the molybdenum atom. The CCDC reference number is 158301.

3.8. DFT calculations

All DFT calculations [10] were performed using the Amsterdam Density Functional program package (ADF) [24]. The Local Spin Density (LSD) exchange correlation potential was used with the Local Density Approximation of the correlation energy (Vosko–Wilk–Nusair) [35].

Gradient corrected geometry optimisations [36] were performed using the Generalised Gradient Approximation (Becke's exchange [37] and Perdew's [38a,b] correlation functionals, and also with Perdew–Wang [38c] exchange and correlation corrections), and included relativistic effects, treated by a quasi-relativistic method where Darwin and mass–velocity terms are incorporated [39].

Unrestricted calculations were performed for all the paramagnetic species studied. The inner shells of W ([1–5]s, [2–5]p, [3–4]d), Mo ([1–4]s, [2–4]p, 3d), Ti ([1–3]s, 2p), Cr ([1–3]s, 2p), C (1s), O (1s), N (1s), Cl (1s, 2s, 2p) were frozen. An uncontracted triple-ζ nd, (n + 1)s STO basis set was used for W, Mo, Ti, and Cr augmented by one (n + 1)p function. The valence shells for C, N, O (2s,2p), and Cl (3s, 3p) were described by an uncontracted triple-ζ STO basis set, augmented by two polarisation functions: 3d and 4f. For H an uncontracted triple-ζ STO basis set (1s) with two polarisation functions 2p and 3d was used. The full geometry optimisations were performed without any symmetry constraints. Time dependent DFT calculations (TD-DFT) [27] were used to determine the excitation energies. In all cases, the lowest ten singlet–singlet excitation energies were calculated using the optimised geometry.

Acknowledgements

This work was financially supported by PRAXIS XXI under project 2/2.1/QUI/316/94. CAG and JPL thank PRAXIS XXI for the grants. EH, MJC, and SCMCG thank the TMR Metal Clusters in Catalysis and Organic Synthesis.

References

[1] (a) A.R. Dias, M.L.H. Green, Chem. Commun. (1969) 962;
(b) A.R. Dias, M.L.H. Green, Rev. Port Quim. 11 (1969) 61;
(c) A.R. Dias, M.L.H. Green, J. Chem. Soc. A (1971) 1951;
(d) A.R. Dias, M.L.H. Green, J. Chem. Soc. A (1971) 2807;
(e) D.W. Stephan, Coord. Chem. Rev. 95 (1989) 41;
(f) R.T. Baker, T.E. Glassman, D.W. Ovenall, J.C. Calabrese, Isr. J. Chem. 31 (1991) 33;
(g) H. Vahrenkamp, A. Geiß, G.N. Richardson, J. Chem. Soc. Dalton Trans. (1997) 3643;
(h) W.P. Fehlhammer, M. Fritz, Chem. Rev. 93 (1993) 1243;
(i) F. Scandola, R. Argazzi, C.A. Bignozzi, C. Chiorboli, M.T. Indelli, M.A. Rampi, Coord. Chem. Rev. 125 (1993) 283.

[2] (a) C.C. Romão, PhD Thesis, Instituto Superior Técnico, Lisboa, 1979;
(b) M.J. Calhorda, PhD Thesis, Instituto Superior Técnico, Lisboa, 1980;
(c) F.J.S. Pina, PhD Thesis, Instituto Superior Técnico, Lisboa, 1982;
(d) M.J. Calhorda, A.M. Galvão, in: M. Gielen (Ed.), Topics in Physical Organometallic Chemistry, Freund Publishing House, Tel-Aviv, 1992, pp. 93–138;
(e) C.C. Romão, Appl. Organomet. Chem. 14 (2000) 1–10.

[3] (a) M.G.B. Drew, V. Félix, I.S. Gonçalves, F.E. Kühn, A.D. Lopes, C.C. Romão, Polyhedron 17 (1998) 1091;
(b) I.S. Gonçalves, F.E. Kühn, A.D. Lopes, A.J. Parola, F. Pina, J. Sotomayor, C.C. Romão, J. Organomet. Chem. 560 (1998) 117;
(c) F.E. Kühn, I.S. Gonçalves, A.D. Lopes, J.P. Lopes, C.C. Romão, W. Wachter, J. Mink, L. Hajba, A.J. Parola, F. Pina, J. Sotomayor, Eur. J. Inorg. Chem. 2 (1999) 295.

[4] P. Braunstein, D. Cauzzi, D. Kelly, M. Lanfranchi, A. Tiripicchio, Inorg. Chem. 32 (1993) 3373.

[5] H. Kunkely, A. Vogler, Inorg. Chim. Acta 254 (1997) 195.

[6] (a) J.R. Ascenso, C.G. de Azevedo, I.S. Gonçalves, E. Herdtweck, D.S. Moreno, M. Pessanha, C.C. Romão, Organometallics 14 (1995) 3901;
(b) M.G.B. Drew, V. Felix, I.S. Gonçalves, C.C. Romão, B. Royo, Organometallics 17 (1998) 5782;
(c) C.A. Gamelas, E. Herdtweck, J.P. Lopes, C.C. Romão, Organometallics 18 (1999) 506;
(d) M.J. Calhorda, C.A. Gamelas, C.C. Romão, L.F. Veiros, Eur. J. Inorg. Chem. (2000) 331;
(e) I.S. Gonçalves, C.C Romão, J. Organomet. Chem. 48 (1995) 155;
(f) I.S. Gonçalves, E. Herdtweck, C.C. Romão, B. Royo, J. Organomet. Chem. 580 (1999) 169;
(g) M.J. Calhorda, I.S. Gonçalves, E. Herdtweck, C.C. Romão, B. Royo, L.F. Veiros, Organometallics 18 (1999) 3956.

[7] W.E. Douglas, M.L.H. Green, J. Chem. Soc. D (1972) 1796.

[8] A.C. Filippou, A.R. Dias, A.M. Martins, C.C. Romão, J. Organomet. Chem. 455 (1993) 129.
[9] E.W. Abel, F.G.A. Stone, G. Wilkinson (Eds.), Comprehensive Organometallic Chemistry II, vol. 10, Oxford, UK, Pergamon Press, 1995 (chap. 4).
[10] R.G. Parr, W. Young, Density Functional Theory of Atoms and Molecules, Oxford University Press, New York, 1989.
[11] H. Willner, F. Aubke, Angew. Chem. Int. Ed. Engl. 36 (1997) 2402.
[12] (a) C.A. Bignozzi, R. Argazzi, J.R. Schoonover, K.C. Gordon, R.B. Dyer, F. Scandola, Inorg. Chem. 31 (1992) 5260;
(b) S. Zhan, X. Chen, G. Meng, Transition Met. Chem. 21 (1996) 181.
[13] K. Clauss, H. Bestian, Leibigs Ann. Chemie 654 (1962) 8.
[14] B. Heyn, B. Hipler, G. Kreisel, H. Schreer, D. Walther, Anorganische Synthesechemie, Springer, Berlin, 1990, p. 81.
[15] A.L. Spek, PLATON, a Multipurpose Crystallographic Tool, Utrecht University, Utrecht, The Netherlands, 1999.
[16] F.H. Allen, J.E. Davies, J.J. Galloy, O. Johnson, O. Kennard, C.F. Macrae, E.M. Mitchell, G.F. Mitchel, J.M. Smith, D.G. Watson, J. Chem. Inf. Comput. Sci. 31 (1991) 187.
[17] D.S. Frohnapfel, S. Reinartz, P.S. White, J.L. Templeton, Organometallics 17 (1998) 3759.
[18] H.M. Dawes, M.B. Hursthouse, A.A. Del Paggio, E.L. Muetterties, A.W. Parkins, Polyhedron 4 (1985) 379.
[19] V.G. Albano, L. Busetto, C. Castellari, M. Monari, A. Palazzi, V.J. Zanotti, Chem. Soc. Dalton Trans. (1993) 3661.
[20] A.K. Sra, M. Andruh, O. Kahn, S. Golhen, L. Ouahab, J.V. Yakhmi, Angew. Chem. Int. Ed. Engl. 38 (1999) 2606.
[21] D.J. Darensbourg, J.C. Yoder, M.W. Holtcamp, K.K. Klausmeyer, J.H. Reibenspies, Inorg. Chem. 35 (1996) 4764.
[22] A.J. Carmichael, A. McCamley, J. Chem.Soc. Dalton Trans. (1995) 3125.
[23] A.J. Carmichael, A. McCamley, J. Chem. Soc. Dalton Trans. (1997) 93.
[24] (a) E.J. Baerends, A. Bérces, C. Bo, P.M. Boerrigter, L. Cavallo, L. Deng, R.M. Dickson, D.E. Ellis, L. Fan, T.H. Fischer, C. Fonseca Guerra, S.J.A. van Gisbergen, J.A. Groeneveld, O.V. Gritsenko, F.E. Harris, P. van den Hoek, H. Jacobsen, G. van Kessel, F. Kootstra, E. van Lenthe, V.P. Osinga, P.H.T. Philipsen, D. Post, C.C. Pye, W. Ravenek, P. Ros, P.R.T. Schipper, G. Schreckenbach, J.G. Snijders, M. Sola, D. Swerhone, G. te Velde, P. Vernooijs, L. Versluis, O. Visser, E. van Wezenbeek, G. Wiesenekker, S.K. Wolff, T.K. Woo, T. Ziegler, ADF, 1999;
(b) C. Fonseca Guerra, O. Visser, J.G. Snijders, G. teVelde, E.J. Baerends, Parallelisation of the Amsterdam Density Functional Programme, in: E. Clementi, C. Corongiu (Eds.), Methods and Techniques for Computational Chemistry, STEF, Cagliari, 1995, pp. 303–395;
(c) C. Fonseca Guerra, J.G. Snijders, G. te Velde, E.J. Baerends, Theor. Chem. Assoc. 99 (1998) 391;
(d) E.J. Baerends, D. Ellis, P. Ros, Chem. Phys. 2 (1973) 41;
(e) E.J. Baerends, P. Ros, Int. J. Quantum Chem. S 12 (1978) 169;
(f) P.M. Boerrigter, G. te Velde, E.J. Baerends, Int. J. Quantum Chem. 33 (1988) 87;
(g) G. te Velde, E.J. Baerends, J. Comp. Phys. 99 (1992) 84.
[25] (a) M.J. Calhorda, L.F. Veiros, Coord. Chem. Rev. 185 (1999) 37;
(b) M.E. Stoll, P. Belanzoni, M.J. Calhorda, M.G.B. Drew, V. Félix, W.J. Geiger, C.A. Gamelas, I.S. Gonçalves, C.C. Romão, L.F. Veiros, submitted.
[26] J.W. Lauher, R.J. Hoffmann, J. Am. Chem. Soc. 98 (1976) 1729.
[27] (a) S.J.A. van Gisbergen, J.A. Groeneveld, A. Rosa, J.G. Snijders, E.J. Baerends, J. Phys. Chem. A 103 (1999) 6835;
(b) A. Rosa, E.J. Baerends, S.J.A. van Gisbergen, E. van Lenthe, J.A. Groeneveld, J.G. Snijders, J Am. Chem. Soc. 121 (1999) 10356;
(c) E.S.J.A. van Gisbergen, A. Rosa, G. Ricciardi, E.J. Baerends, J. Chem. Phys. 111 (1999) 2499.
[28] J.C. Kotz, W. Vining, W. Coco, R. Rosen, A.R. Dias, M.H. Garcia, Organometallics 2 (1982) 68.
[29] (a) N. Zhu, H. Vahrenkamp, Angew. Chem. Int. Ed. Engl. 33 (1994) 2090;
(b) C.A. Bignozzi, S. Roffia, F. Scandola, J. Am. Chem. Soc. 107 (1985) 1644.
[30] I.V. Nelson, R.T. Iwamoto, Anal. Chem. 35 (1963) 867.
[31] R.B. King, Inorg. Chem. 6 (1967) 25.
[32] W. Kabsch, J. Appl. Crystallogr. 21 (1988) 916.
[33] N. Walker, Stuart, DIFABS, Acta Crystallogr. A 39 (1983) 158.
[34] G.M. Sheldrick, SHELX-97, University of Göttingen, 1997.
[35] S.H. Vosko, L. Wilk, M. Nusair, Can. J. Phys. 58 (1980) 1200.
[36] (a) L. Versluis, T. Ziegler, J. Chem. Phys. 88 (1988) 322;
(b) L. Fan, T.J. Ziegler, Chem. Phys. 95 (1991) 7401.
[37] (a) A.D. Becke, J. Chem. Phys. 88 (1987) 1053;
(b) A.D. Becke, Phys. Rev. A 38 (1988) 3098.
[38] (a) J.P. Perdew, Phys. Rev. B 33 (1986) 8822;
(b) J.P. Perdew, Phys. Rev. B 34 (1986) 7406;
(c) J.P. Perdew, J.A. Chevary, S.H. Vosko, K.A. Jackson, M.R. Pederson, D.J. Singh, C. Fiolhais, Phys. Rev. B 46 (1992) 6671.
[39] (a) T. Ziegler, V. Tschinke, E.J. Baerends, J.G. Snijders, W. Ravenek, J. Phys. Chem. 93 (1989) 3050;
(b) J.G. Snijders, E.J. Baerends, Mol. Phys. 36 (1978) 1789;
(c) J.G. Snijders, E.J. Baerends, P. Ros, Mol. Phys. 38 (1979) 1909;
(d) A. Rosa, E.J. Baerends, S.J.A. van Gisbergen, E. van Lenthe, J.A. Groeneveld, J.G. Snijders, J Am. Chem. Soc. 121 (1999) 10358.